Self-organization of atoms in a cavity field: Threshold, bistability, and scaling laws

J. K. Asbóth,[1,2] P. Domokos,[1] H. Ritsch,[2] and A. Vukics[1]
[1]*Research Institute of Solid State Physics and Optics, Hungarian Academy of Sciences, H-1525 Budapest P.O. Box 49, Hungary*
[2]*Institute of Theoretical Physics, University of Innsbruck, Technikerstrasse 25, A-6020 Innsbruck, Austria*
(Received 18 July 2005; published 30 November 2005)

We present a detailed study of the spatial self-organization of laser-driven atoms in an optical cavity, an effect predicted on the basis of numerical simulations [P. Domokos and H. Ritsch, Phys. Rev. Lett. **89**, 253003 (2002)] and observed experimentally [A. T. Black *et al.*, Phys. Rev. Lett. **91**, 203001 (2003)]. Above a threshold in the driving laser intensity, from a uniform distribution the atoms evolve into one of two stable patterns that produce superradiant scattering into the cavity. We derive analytic formulas for the threshold and critical exponent of this phase transition from a mean-field approach. Numerical simulations of the microscopic dynamics reveal that, on a laboratory time scale, a hysteresis masks the mean-field behavior. Simple physical arguments explain this phenomenon and provide analytical expressions for the observable threshold. Above a certain density of the atoms a limited number of "defects" appear in the organized phase and influence the statistical properties of the system. The scaling of the cavity cooling mechanism and the phase-space density with the atom number is also studied.

DOI: 10.1103/PhysRevA.72.053417 PACS number(s): 32.80.Pj, 42.50.Fx, 42.50.Vk, 68.18.Jk

I. INTRODUCTION

The manipulation of cold atoms and molecules by laser light is a rapidly growing field and has become a suitable ground for studying fundamental phenomena of physics both experimentally and theoretically [1]. In the last decade, the emphasis has partly been shifted towards many-body effects in the dynamics of weakly interacting atoms [2,3]. The mechanical action of the electromagnetic radiation field on free atoms rarely manifests these effects. The refractive index of a cloud of atoms is simply composed of the product of the single-atom polarizability and the optical density. Standard laser cooling methods were also conceived on the basis of single-atom processes. Only at densities as high as the ones achievable in a magneto-optical trap does the dipole-dipole interaction between atom pairs give rise to a Lorentz-Lorenz-type refractive index and present an appreciable nonlinearity in the optical density [4,5]. The underlying process, the reabsorption of spontaneously scattered photons in the atomic cloud [6,7], heats the atomic motion and hence limits the attainable minimum temperature. In addition, this effect also introduces spatial instability into the atomic cloud and thus hinders degeneracy in phase space by optical means [8].

The mechanical effect of light on atoms inside a high-finesse resonator is substantially modified with respect to free space, which is the source of a variety of interesting phenomena in optical cavity quantum electrodynamics [9,10]. The basic reason is that a cavity photon makes many round-trips between the mirrors and thus the back action of the atom on the field, enhanced by the cavity finesse, cannot be neglected. As opposed to the external forces exerted by laser fields, the light forces in a cavity cannot be separated from the dynamics of the resonator mode, which is strongly influenced by that of the atom.

The coupled atom-field dynamics can yield an efficient damping of the atomic motion via the mirror loss dissipation channel [11,12]. Such "cavity cooling" schemes have recently been demonstrated experimentally [13,14]. The fact that cavity cooling allows for replacing the spontaneous emission, which is the dissipation channel in all laser cooling schemes, by irreversible photon loss from the cavity has important consequences. First, the internal structure of the atom is not important and the mechanism can be operated on a wide range of species. Second, the problem of the reabsorption of spontaneously scattered photons, the source of the instability of atomic clouds at high densities, can be suppressed.

The dynamics of atoms in a resonator is inherently a many-body problem even at a small density of the ensemble [15,16]. As all atoms are coupled to the same cavity mode, the modification of the field by one atom is experienced by a remote atom as well as by itself. The cavity cooling mechanism may become inefficient since the delicate dynamical correlation between one atom and the field mode could be perturbed by the motion of another atom [17,18]. Indeed, one of the cavity cooling schemes was found to slow down linearly with increasing number of atoms [19].

In a recent Letter we predicted a cooperative behavior of the atoms driven by a laser in a direction perpendicular to the axis of a standing-wave cavity [20]. At high pump laser intensities (above a threshold) the homogeneous atomic cloud self-organizes into one of two regular checkerboard patterns that maximize scattering into the cavity. The constructive interference of fields radiated by the individual atoms produces an intensity which depends quadratically on the number of atoms (superradiance). Corresponding to the two patterns, there are two possible phases of the output field with 180° difference, which have been observed in an experiment by Black, Chan, and Vuletić [21].

The onset of self-organization is relatively fast, on the microsecond time scale. A basic property of the present system is that the field created by the atoms traps and simultaneously cools them so that the organized pattern remains stable on a long time scale (tens of ms). The cavity cooling mechanism now acts on many atoms without losing efficiency. There is no external finite-temperature heat bath to

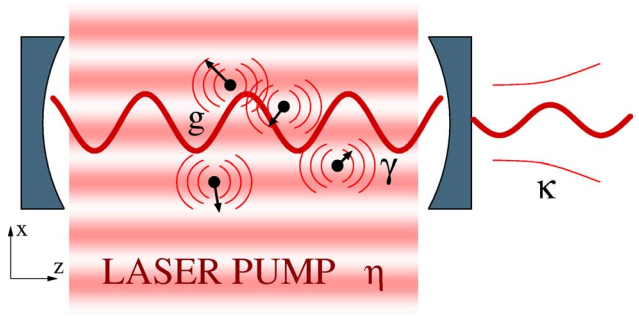

FIG. 1. (Color online) The setup: transversely driven atoms moving in a standing-wave cavity. The laser intensity is given by the maximum free-space Rabi frequency (pumping strength) η. The atoms couple to the cavity mode with one-photon Rabi frequency g. The loss channels are spontaneous emission (rate 2γ) and cavity loss (rate 2κ).

define the temperature which, instead, is set by the dynamical equilibrium of the dipole force fluctuations and the cavity cooling effect. This is a distinctive feature with respect to the recently demonstrated collective atomic recoil laser in a ring cavity (CARL) [22–25], where a magneto-optical trap is necessary to stabilize the organized phase, and the otherwise transient gain [26], and also to inject noise for obtaining the phase-transition-like behavior [27–31].

In the present paper we discuss in detail the self-organization process from the viewpoint of phase transitions. A mean-field approach leads to a well-defined threshold in the pumping strength. Comparison to numerical simulations reveals effects scaling unusually with the atom density, a characteristic feature of this cavity-coupled many-atom system.

The paper is organized as follows. In Sec. II, the equations of a semiclassical model are recapitulated, where the atoms are represented as simple linearly polarizable particles. Thereby the theory applies to a much wider class of particles than alkali-metal atoms. The main features of the self-organization process, such as time scales, superradiance, and collective cooling, are surveyed using a numerical example in Sec. III. Then, in Sec. IV, we introduce a one-dimensional mean-field model and determine the threshold and critical exponent. In Sec. V, we present the results of detailed numerical simulations, which show effects beyond the mean field. The atom number enters the physics of the system in a form other than the density. Above a certain atom number, stable defects appear in the self-organized pattern and modify the system properties, which is accounted for in Sec. VI. In Sec. VII, the cooperative atomic behavior is discussed in detail by demonstrating the superradiance and the ensuing improvement of localization by collectivity. We conclude in Sec. VIII.

II. SEMICLASSICAL MODEL

We consider N atoms in an open optical resonator (Fig. 1). The atoms are illuminated from the side by a "transverse" standing-wave laser pump with frequency ω. This geometry corresponds to various experimental setups realizing the controlled transport of atoms from the side into a cavity [14,32] where the standing-wave pump amounts to a "conveyor belt" [33,34]. There is an efficient scattering of photons into the cavity mode quasiresonant with the pump, $\omega_C \approx \omega$, due to the enhanced dipole coupling described by the single-photon Rabi frequency $g=\omega_C^{1/2}[2\epsilon_0\hbar V]^{-1/2}d_{eg}$, for a mode volume V and atomic transition dipole moment d_{eg} along the cavity mode polarization. Large detuning of the laser from the atomic transition $|\omega-\omega_A| \gg \gamma$, where 2γ is the full atomic linewidth at half maximum, ensures that the upper level of the atoms can be adiabatically eliminated. This model then describes a very general class of linearly polarizable particles—in the following, we continue to use "atoms" for convenience. For the sake of simplicity, we restrict the atomic motion to two dimensions, along the pump laser and the cavity axis, coordinates x and z, respectively, without losing any relevant physical effect. Motion in the third dimension could be taken into account in the same way as along x.

The quantum master equation for the density matrix reads

$$\dot{\rho} = -\frac{i}{\hbar}[H,\rho] + \mathcal{L}\rho. \tag{1}$$

Here the Hamiltonian is

$$H = \sum_{j=1}^{N} \frac{\mathbf{p}_j^2}{2M} - \hbar\Delta_C a^\dagger a + \hbar U_0 \sum_{j=1}^{N} E^\dagger(\mathbf{r}_j)E(\mathbf{r}_j), \tag{2a}$$

where a and $a^\dagger$ are the boson operators of the cavity mode, and $\mathbf{r}_j=(x_j,z_j)$ and $\mathbf{p}_j=(p_{x_j},p_{z_j})$ are the position and momentum vectors of the jth atom. The Liouville operator describing the cavity photon losses with rate 2κ and the spontaneous emission reads

$$\begin{aligned}\mathcal{L}\rho = {} & 2\kappa\left(a\rho a^\dagger - \frac{1}{2}a^\dagger a\rho - \frac{1}{2}\rho a^\dagger a\right) \\ & - \Gamma_0 \sum_{j=1}^{N} \left(E^\dagger(\mathbf{r}_j)E(\mathbf{r}_j)\rho + \rho E^\dagger(\mathbf{r}_j)E(\mathbf{r}_j) \right. \\ & \left. - 2\int d^2\mathbf{u} N(\mathbf{u}) E(\mathbf{r}_j) e^{-ik_A \mathbf{u}\mathbf{r}_j} \rho e^{ik_A \mathbf{u}\mathbf{r}_j} E^\dagger(\mathbf{r}_j) \right).\end{aligned} \tag{2b}$$

In the above formulas, $E(\mathbf{r})$ is the dimensionless electric field,

$$E(\mathbf{r}) = f(\mathbf{r})a + \eta(\mathbf{r})/g \approx \cos(kz)a + \cos(kx)\,\eta/g. \tag{2c}$$

The Rabi frequency of the driving laser is $\eta(\mathbf{r})$, whose position dependence is given by a $\cos(kz)$ mode function for a standing-wave field. In the following, we are going to refer to the maximum value of the Rabi frequency η as "pumping strength." The variation of the pump field along the cavity axis and that of the cavity mode function $f(\mathbf{r})$ along the transverse direction (Gaussian envelope) are neglected. The detunings are defined as $\Delta_C=\omega-\omega_C$ and $\Delta_A=\omega-\omega_A$. The parameters

$$U_0 = \frac{g^2\Delta_A}{\Delta_A^2+\gamma^2}, \quad \Gamma_0 = \frac{g^2\gamma}{\Delta_A^2+\gamma^2} \tag{3}$$

describe the dispersive and absorptive effects of the atoms, respectively, as they shift and broaden the resonance line of the cavity. In the last term of Eq. (2b), the integral represents the averaging over the angular distribution $N(\mathbf{u})$ of the random recoil due to spontaneous emission into the free-space modes.

Instead of directly using the density matrix, we consider the evolution of the corresponding joint atom-field Wigner function [35]. This can be systematically approximated by semiclassical equations for a set of classical stochastic variables α, $\mathbf{p}_j$, and $\mathbf{r}_j$, the index $j=1,\ldots,N$ labeling the atoms,

$$\dot{\alpha} = i\left[\Delta_C - U_0\sum_j \cos^2(kz_j)\right]\alpha - \left[\kappa + \Gamma_0\sum_j \cos^2(kz_j)\right]\alpha - \eta_{\text{eff}}\sum_j \cos(kz_j)\cos(kx_j) + \xi_\alpha, \tag{4a}$$

$$\dot{p}_{x_j} = -\hbar U_0(\eta/g)^2\frac{\partial}{\partial x_j}\cos^2(kx_j) - i\hbar(\eta_{\text{eff}}^*\alpha - \eta_{\text{eff}}\alpha^*)\frac{\partial}{\partial x_j}\cos(kx_j)\cos(kz_j) + \xi_{x_j}, \tag{4b}$$

$$\dot{p}_{z_j} = -\hbar U_0|\alpha|^2\frac{\partial}{\partial z_j}\cos^2(kz_j) - i\hbar(\eta_{\text{eff}}^*\alpha - \eta_{\text{eff}}\alpha^*)\frac{\partial}{\partial z_j}\cos(kx_j)\cos(kz_j) + \xi_{z_j}, \tag{4c}$$

where the effective pumping strength for the cavity mode is

$$\eta_{\text{eff}} = \frac{\eta g}{-i\Delta_A + \gamma}. \tag{5}$$

These equations include Langevin noise terms ξ_α, ξ_{x_j}, and ξ_{z_j}, defined by the nonvanishing second-order correlations

$$\langle \xi_\alpha^*\xi_\alpha\rangle = \kappa + \sum_{j=1}^{N}\Gamma_0\cos^2(kz_j), \tag{6a}$$

$$\langle \xi_n\xi_\alpha\rangle = i\hbar\Gamma_0\partial_n\mathcal{E}(\mathbf{r}_j)\cos(kz_j), \tag{6b}$$

$$\langle \xi_n\xi_m\rangle = 2\hbar^2k^2\Gamma_0|\mathcal{E}(\mathbf{r}_j)|^2\overline{u_n^2}\delta_{nm} + \hbar^2\Gamma_0[\partial_n\mathcal{E}^*(\mathbf{r}_j)\partial_m\mathcal{E}(\mathbf{r}_j) + \partial_n\mathcal{E}(\mathbf{r}_j)\partial_m\mathcal{E}^*(\mathbf{r}_j)], \tag{6c}$$

where the indices $n,m=x_j,z_j$. The noise terms associated with different atoms are not correlated. The complex dimensionless electric field $\mathcal{E}(\mathbf{r})$ is derived from Eq. (2c), replacing the field operator a by the complex variable α. We iterate the coupled, stochastic Ito-type differential equations (4) by a Monte Carlo–type algorithm.

There are two types of force terms in the equations of the momentum components. The terms in the first lines derive from the usual one-dimensional "optical lattice" potentials; the laser pump keeps the atoms inside the resonator via this term. In the second lines, the force terms originate from the coherent redistribution of photons between the pump and field mode. The potentials depending on the amplitude α, which itself is a variable, are not conservative (all but the optical lattice created by the transverse pump). The time-delayed correlations in the dynamics of the atomic motion and the field mode can result in a friction force on the atoms, known as cavity cooling [11,35–41].

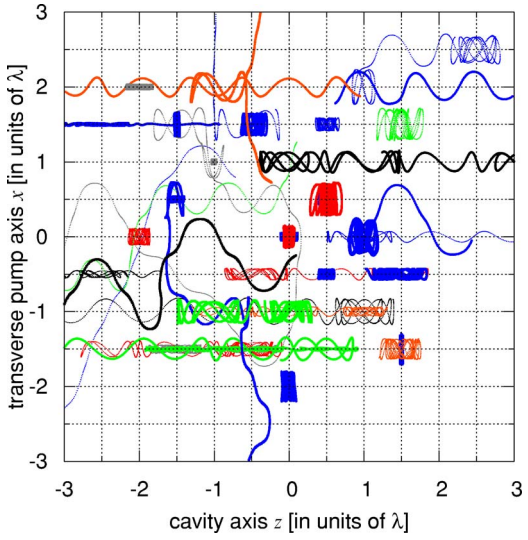

FIG. 2. (Color online) Two-dimensional trajectories of 40 rubidium atoms in a cavity, during the initial 50 μs. A checkerboard pattern of trapped atoms emerges; untrapped atoms move mainly along the cavity axis. Parameters: $\gamma=20/\mu$s, $(g,\kappa)=(2.5,0.5)\gamma$, atomic detuning $\Delta_A=-500\gamma$, cavity detuning $\Delta_C=-\kappa+NU_0$, and the pumping strength $\eta=50\gamma$.

III. SELF-ORGANIZATION

We study he motion of the atoms in the cavity by numerically integrating the set of stochastic ordinary differential equations (4). To be specific, ^{85}Rb was considered, with the $5\,^2S_{1/2},F=3\leftrightarrow 5\,^2P_{3/2},F=4$ transition. Starting from a gas of thermal atoms (random positions from a uniform and velocities from a thermal distribution) and no light in the cavity mode ($\alpha=0$), with the right choice of parameters we observe a buildup of the cavity field accompanied by the appearance of an organized pattern in the spatial distribution of the atoms. This is illustrated in Fig. 2, where the trajectories of 40 atoms during the initial 50 μs of a run are shown. The grid lines denote points of maximum coupling to the standing-wave cavity or pump field. Trapped atoms are oscillating about intersections of grid lines, where a single atom can scatter pump photons into the cavity mode most efficiently. For many atoms, however, destructive interference can inhibit the scattering process: the source term in Eq. (4a) contains the factor $\Sigma_j\cos(kx_j)\cos(kz_j)$, which can be small even if all the atoms are maximally coupled due to the alternating signs of the summands. In contrast to this, in Fig. 2, only every second "maximally coupled" site—the black or the white fields of a checkerboard—is occupied, leading to an

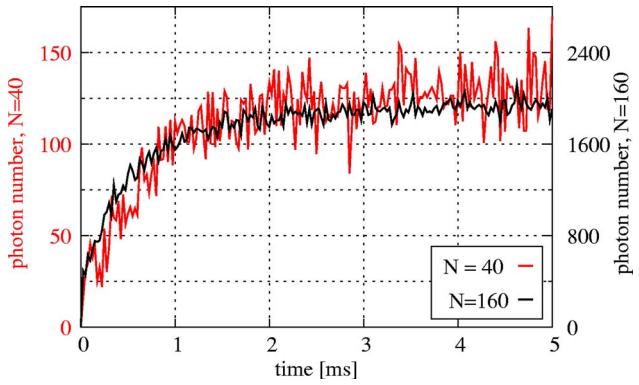

FIG. 3. (Color online) The time evolution of the photon number in the cavity on a long time scale, for $N=40$ and $N=160$ atoms (note the different vertical scaling). The parameters are the same as in Fig. 2

efficient Bragg scattering of pump photons into the cavity.

The emergence of a checkerboard pattern of atoms with every second point of maximum coupling empty happens only due to the good choice of the parameters, ensuring positive feedback, as explained in the following. Initially, in the random position distribution some atoms scatter into the cavity in a given phase and some with an opposite phase, and thus most of the scattered field is canceled. The dipole force [first term of Eq. (4b)] attracts atoms towards antinodes of the pump (for red detuning, $\Delta_A<0$), but almost no field in the cavity means no substantial modification of the uniform position distribution along the cavity axis. This can be seen in Fig. 2, where most atoms are well trapped along the transverse axis but some meander along the cavity axis. Due to statistical fluctuations, either the in-phase or opposite-phase scatterers will be in a tiny majority and a small cavity field does build up. The dipole force due to the cavity field, first term of Eq. (4c), now attracts atoms towards antinodes of the cavity. The crucial point to consider is the interference of the cavity and pump fields, giving the second terms in Eqs. (4b) and (4c). The product $\cos(kx_j)\cos(kz_j)$ alternates sign between the black and white fields of the checkerboard. For a right choice of detuning Δ_C, there is a positive feedback and the atoms are attracted towards the "majority" sites and are repelled from the "minority" sites, due to the interference.

The initial fast buildup continues over a longer time scale, with the kinetic energy of the oscillating and free-flying untrapped atoms dissipated owing to the cavity cooling mechanism (for the transverse pumping case and for the chosen detuning Δ_C, it is the one described in Ref. [36]). This leads to an increase of the ratio of trapped atoms and to a stronger localization in the vicinity of the antinodes. Simultaneously, the coherent scattering into the cavity improves, giving a slow increase in the cavity field intensity. The time evolution of the photon number is plotted in Fig. 3 for this self-organization process of 40 and 160 atoms. In the latter case, the photon number scale was rescaled by a factor of 16. This way, the overlap of the two curves demonstrates the superradiance effect; i.e., the intensity is quadratically proportional to the atom number.

In this phase-transition-like process, the reduction of the kinetic energy is not a good characterization of the cooling

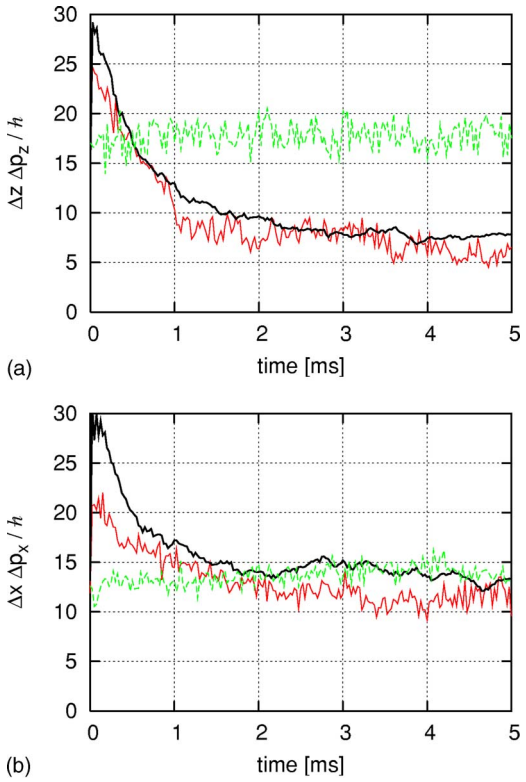

FIG. 4. (Color online) Evolution of the phase-space volume, along the cavity axis (up) and along the transverse pump (bottom), on a long time scale for various settings, the same parameters as in Fig. 3. The number of atoms is $N=40$ and $N=160$ (black line) and $N=40$ but pumped below threshold, $\eta=10\gamma$, for the dashed line.

efficiency. For the motion along the cavity axis, the transition from vanishing photon number to the "superradiated" light field is accompanied by a change of the heat capacity of the atomic ensemble since the number of quadratic degrees of freedom changes from 1 (kinetic energy) to 2 (kinetic and potential energy). In deep harmonic traps, even a very low level of excitation can correspond to high kinetic energies. Thus even though the temperature can increase, cavity-induced dissipation increases the phase-space density of the system by improving localization. An appropriate measure of this process is the effective phase-space volume of the system (the inverse of the phase-space density), measured by the Heisenberg uncertainty product $\Delta x\Delta p_x/\hbar$ and $\Delta z\Delta p_z/\hbar$ for each degree of freedom. Here $(\Delta x)^2$ and $(\Delta z)^2$ are the averages of the squared distance of the atom from the nearest antinode along the directions x and z, respectively. For a harmonic potential, the dimensionless effective phase-space volume amounts precisely to the mean number of excitation quanta. For untrapped atoms with mean kinetic energy $\langle p^2/m\rangle=k_BT$, the phase-space volume is $\lambda\sqrt{mk_BT}/(4\sqrt{3}\hbar)$.

In Fig. 4, the time evolution of the Heisenberg uncertainty product is shown for three cases. When the pumping strength is below threshold ($N=40$, $\eta=10\gamma$), the uncertainty product is a constant. Here the spatial distribution of the atomic ensemble remains uniform—the transverse pump is too weak to induce any noticeable spatial modulation at temperatures $k_BT\approx\hbar\kappa$. Thus $\langle\Delta z\Delta p_z\rangle=$const and $\langle\Delta x\Delta p_x\rangle=$const reveal

that the temperature itself does not change in either direction. At the cavity cooling limit $k_BT=\hbar\kappa$ the numerical value for the phase-space volume from the last paragraph is $13.4\hbar$, in accordance with the value along the transverse x direction. Along the cavity axis z, however, the phase-space volume is above this estimate, indicating a higher temperature. Above threshold, the phase-space volume transiently jumps to high values for both directions and then it is gradually decreased. Compression is apparently more efficient along the cavity axis; here, the phase space goes considerably below the value corresponding to the uniform distribution. In both plots the two curves corresponding to $N=40$ and $N=160$ are very similar, which manifests that the cooling rate of the ensemble is independent of the atom number. This is a very important observation, being at variance with the expectation that the efficiency of cavity cooling mechanism is reduced for increasing number of atoms. This prediction was made for a setup where the external pump field is injected directly into the cavity. Apparently it does not apply to the transverse pumping case studied here.

With the help of these few examples, we surveyed three important properties appearing in the dynamics of a laser-driven atomic ensemble coupled to a cavity mode: (i) the system rapidly self-organizes into a checkerboard pattern in a trapping field, (ii) which is generated by a collective, superradiant scattering into the cavity, and finally, (iii) the energy of the atoms is dissipated at a rate independent of the number of atoms. This behavior requires a sufficiently strong pumping strength, indicating the possibility of a well-defined threshold separating two different stability regions. This threshold is discussed in the next section within the framework of a mean-field approximation.

IV. MEAN-FIELD APPROXIMATION

The essence of the self-organization process can be understood on the ground of conservative mean-field forces acting on the atoms. This amounts to treating the cavity field as if it responded immediately to the positions of the atoms. Cavity cooling, which is directly related to the time lag of the cavity field, is absent in this model. Moreover, the mean-field approach corresponds to the thermodynamic limit of the system: $N\to\infty$, $g\to 0$, $\kappa=$const with $Ng^2=$const. Physically, the limit can be thought of as taking larger cavities (cavity length $l_{\mathrm{cav}}\to\infty$) filled with a gas of atoms of constant density (atom number $N\propto l_{\mathrm{cav}}$). Due to the $V^{-1/2}$ dependence of the coupling constant g on the mode volume V, one then has $Ng^2=$const, neglecting the variation of the waist of the mode. Moreover, due to larger photon travel time between the mirrors, the reflectivity has to scale like $\propto l_{\mathrm{cav}}^{-1}$ to keep $\kappa=$const. For the sake of simplicity, we analyze one-dimensional (1D) motion along the cavity.

A. Potentials

Taking $x_j=0$, $j=1,\ldots,N$, according to Eq. (4c) each atom moves in a potential

$$V(z)=U_2\cos^2(kz)+U_1\cos(kz) \tag{7}$$

composed of the sum of a $\lambda/2$ periodic potential stemming from the cavity field and a λ periodic one arising from the interference between cavity and pump fields. The potential depths are given by

$$U_2=N^2\langle\cos(kz)\rangle^2\hbar I_0U_0, \tag{8a}$$

$$U_1=2N\langle\cos(kz)\rangle\hbar I_0[\Delta_C-NU_0\langle\cos^2(kz)\rangle]. \tag{8b}$$

These, in the mean-field approximation, depend on the position of the individual atoms only via the mean value

$$\Theta=\langle\cos(kz)\rangle=\frac{1}{N}\sum_{i=1}^{N}\cos(kz_i), \tag{9}$$

which can be considered a spatial order parameter, and via the bunching parameter

$$\mathcal{B}=\langle\cos^2(kz)\rangle=\frac{1}{N}\sum_{i=1}^{N}\cos^2(kz_i). \tag{10}$$

The order parameter Θ has characteristic values: (i) $\Theta\approx 0$ describes the uniform distribution, and (ii) $\Theta\to\pm 1$ corresponds to a self-organized phase with atoms in the even or odd antinodes, respectively. Finally, I_0 represents the maximum number of photons each atom can scatter into the cavity

$$I_0=\frac{|\eta_{\mathrm{eff}}|^2}{[\kappa+N\Gamma_0\mathcal{B}]^2+[\Delta_C-NU_0\mathcal{B}]^2}. \tag{11}$$

In equilibrium the spatial distribution of the atoms and the above averages are time independent, which makes it possible to attribute a physical meaning to the potential (7). Since the potential depends on the position distribution, however, the system is highly nonlinear.

For $U_0<0$, obviously $U_2<0$ and the cavity field gives a potential with "even" wells at $kz=2n\pi$ and "odd" ones at $kz=(2n+1)\pi$. The interference term $[\propto\cos(kz)]$ discriminates between the even and odd sites, raising the energy of one of them and lowering that of the other. If $2|U_2|<|U_1|$, this effect is so strong that $V(z)$ yields a potential with wells at the even and hills at the odd sites—or the other way around, depending on the sign of U_1.

The sign of U_1 is crucial. To simplify the dependence, let us require a cavity detuning $\Delta_C<-N|U_0|$ so that the second factor in U_1 is always negative regardless of the momentary configuration of the atoms. To be specific, in the following we are going to use

$$\Delta_C=NU_0-\kappa. \tag{12}$$

If the atoms accumulate around the even (odd) antinodes, then $\Theta\approx+1$ $(\Theta\approx-1)$ and the $U_1\cos kz$ potential is attractive at the even (odd sites), while repulsive at the odd (even) sites. Therefore Eq. (12) is the proper choice for positive feedback that makes the runaway solution of self-organization possible.

Two more parameters describing spatial order are used later in this work: (i) the "defect ratio," the ratio of atoms closer to minority sites than majority sites; and (ii) the "localization parameter," the position variance (along the cavity axis and/or the transverse pump):

$$\mathcal{D}_z = \frac{1}{N}\sum_{i=1}^{N}\left(\frac{kz_i}{\pi}\right)^2, \tag{13}$$

where z_i is measured from the nearest antinode of the cavity mode function. A uniform distribution of atoms gives a defect ratio close to 50% and a localization parameter of 1/12. For a self-organized pattern, both parameters approach 0.

B. Canonical distribution

We suppose that the phase-space distribution of the atoms factorizes to position and momentum dependence, the latter simply given by a thermal distribution with mean energy k_BT. There is no external finite-temperature heat bath to set k_BT; it is instead determined by the dynamics (4) through the equilibrium of the cavity cooling and the Langevin noise terms. This allows for a position- and time-dependent effective temperature, effects neglected in this model. For a far-detuned pump, cavity losses dominate spontaneous emission and an estimate $k_BT \approx \hbar\kappa$ is provided by the Einstein relation. The spatial density of the atoms in the potential $V(z)$ is then given by a canonical distribution

$$\rho(z) = \frac{1}{Z}\exp[-V(z)/(k_BT)], \tag{14}$$

with the partition function $Z=\int \exp[-V(z)/(k_BT)]dz$ ensuring that $\rho(z)$ is normalized to unity. In our case the potential $V(z)$ is a function of the density $\rho(z)$; therefore, this equation has to be solved in a self-consistent manner.

A direct approach to solving Eq. (14) is to use it iteratively to determine the $\rho(z)$ for given values of the physical parameters. We set the temperature to the cavity cooling limit $k_BT=\hbar\kappa$. Note that the temperature parameter T just rescales the pumping strength η; e.g., taking $k_BT=2\hbar\kappa$ would correspond to increasing η by a factor of $\sqrt{2}$. The results thus obtained after 100 iterations of Eq. (14) for an experimentally realistic example are shown in Fig. 5 (open diamonds). There we plot the percentage of atoms near odd sites—i.e., with $|(2m+1)\lambda/2-z|<\lambda/4$ for any integer m—as a function of the pumping strength. Below a certain threshold in the pumping laser amplitude η^* (vertical dotted line) the atoms are distributed uniformly; for stronger pumping, this symmetry is broken. Two examples of such self-organized position distributions obtained by the iterations are shown in the insets. Note also that the convergence of the iterations is slow near the critical η^* (critical slowing down); this is evidenced by plotting the results after 10 iterations (solid circles) as well.

The uniform distribution $\rho(z)=1/\lambda$ leads to $\Theta=0$, $\mathcal{B}=1/2$, which give $V(z)=0$; thus, the distribution fulfills Eq. (14) trivially for any values of the physical parameters. To investigate its stability, we add an infinitesimal perturbation to it,

$$\rho^{(0)}(z) = \frac{1}{\lambda} + \epsilon g(z)\frac{1}{\lambda}, \tag{15}$$

with ϵ infinitesimal, and the general λ-periodic perturbation function

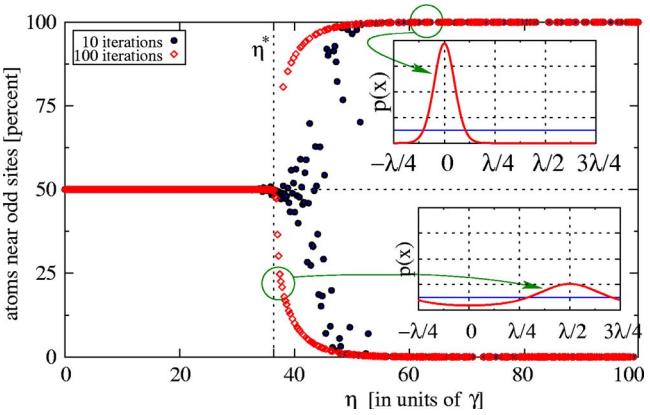

FIG. 5. (Color online) Numerical iterations of the mean-field approximation. The percentage of atoms near odd sites after 10 (solid circles) and 100 (open diamonds) iterations is shown varying the pumping strength η. The vertical line is at η^* of Eq. (19). The two insets show two steady-state position distribution functions at two different pumping strengths. Parameters: $\kappa=\gamma/2$, $\Delta_A=-500\gamma$, $Ng^2=200\gamma^2$, $\Delta_C=-\kappa-Ng^2/|\Delta_A|$, and $k_BT=\hbar\kappa$.

$$g(z) = \sum_{m=1}^{\infty}[A_m\cos(mkz) + B_m\sin(mkz)],$$

$$\sum_m A_m^2 + B_m^2 = 1. \tag{16}$$

Since the spatial average of $g(z)$ disappears, $\rho^{(0)}(z)$ is normalized to 1. Iterating Eq. (14) once leads to the new density function

$$\rho^{(1)}(z) = \frac{1}{\lambda} - N\epsilon\frac{A_1}{\lambda}\frac{\hbar I_0}{k_BT}\left(\Delta_C - \frac{N}{2}U_0\right)\cos(kz) + o(\epsilon^2). \tag{17}$$

To lowest order in ϵ the only relevant perturbation is that proportional to $\cos kz$. Stability requires that the first-order correction in ϵ be self-contracting. Substituting Eq. (12) for the cavity detuning, we have the following instability threshold for the uniform distribution:

$$NI_0\hbar\left(\frac{N}{2}|U_0| + \kappa\right) > k_BT. \tag{18}$$

For far-detuned atoms $|\Delta_A| \gg Ng^2/\kappa$; i.e., when the total cavity mode shift by the atoms is much smaller than the cavity linewidth, $N|U_0| \ll \kappa$. This translates into the following threshold on the pumping strength:

$$\eta > \eta^* = \sqrt{\frac{k_BT}{\hbar\kappa}}\frac{\kappa|\Delta_A|}{\sqrt{N}g}\sqrt{2}. \tag{19}$$

This approximation of the critical value η^* is in good agreement with the simulations shown on Fig. 5, giving $\eta^*=35.4\gamma$, which differs by less than γ from the actual value. To make the physical content more transparent, this condition can be expressed in terms of the transverse pumping power density (energy/unit area/unit time) as

$$P_{\text{in}} > k_B T \left(\frac{\Delta_A}{\gamma}\right)^2 \kappa \frac{4k^3}{3N/V}. \tag{20}$$

As shown in the next section, the condition (19) amounts to requiring that the potential depth along the cavity axis of a self-organized checkerboard pattern exceed significantly the energy scale of thermal fluctuations.

C. Critical exponent

The stability analysis of the uniform distribution of atoms $\rho(z)=1/\lambda$ has revealed the critical value of the pumping strength η^*. Moreover, we have seen that for $\eta \approx \eta^*$, the relevant perturbation gives

$$\rho(z) = 1/\lambda + \epsilon \cos(kz)/\lambda. \tag{21}$$

Going beyond first-order perturbations, the above formula allows us to solve Eq. (14) self-consistently.

Pumping the atoms slightly above threshold, $\eta=\eta^*(1+\delta)$, with $\delta \ll 1$, we expect Eq. (21) to give a good approximation of $\rho(z)$, with ϵ depending nonlinearly on δ. Substituting it into Eq. (14) we need to expand the exponential to third order to obtain a solution to lowest order in the small parameters. This analytical calculation yields $\epsilon \propto \delta^{1/2}$; i.e., above the critical value, ϵ increases from 0 as the square root of the dimensionless excess pumping strength. The order parameter $\theta=\epsilon/2$ and the percentage of majority atoms $(2\epsilon/\pi)$ both depend linearly on the small parameter ϵ. Therefore, the analytical result shows the critical exponent of this phase transition to be $\frac{1}{2}$.

V. NUMERICAL SIMULATIONS OF THE PHASE TRANSITION

In the mean-field description of the steady state, the number of atoms enters only in the form of the atomic density $N/V \propto Ng^2$. The approximation is expected to be valid in the thermodynamic limit—i.e., $N \to \infty$ with the atomic density and the cavity loss rate constant. Trying to approach this limit in simulations of Eq. (4) we are in for a surprise. In Fig. 6, we show the measured percentage of defect atoms after 4 ms of simulation time as a function of the pumping laser strength. The thermodynamic limit is approached in three steps: $N=50$, 200, and 800. The parameters are the same as in Fig. 5; the atoms had random initial velocities from a thermal distribution with average kinetic energy $\hbar\kappa$. The initial positions were either uniformly distributed ("up") or at "odd" points of maximal coupling ("down"). In this controlled way we mimic the ramping of the laser power. Although the "down" curves show reasonable agreement with the mean-field result, the "up" curves scale anomalously: a hysteresis is observed, whose breadth increases with the atom number.

The hysteresis effect observed in Fig. 6 but absent from the mean-field prediction is due to the long time scales associated with reaching a steady state. In fact, thermal fluctuations do not only alter the equilibrium solution by smoothing out the concentration differences due to the dynamics (this is correctly rendered by the mean-field approach), but they can also delay significantly the onset of that equilibrium. This slowing down is effective if the energy scale of thermal fluctuations is at least of the same order as the potential diffences due to the statistical fluctuations in the initial positions of the atoms.

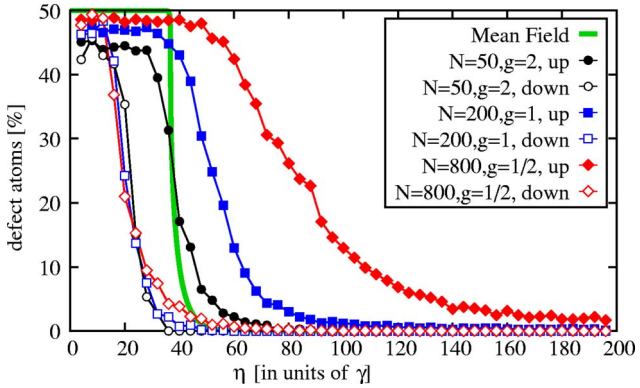

FIG. 6. (Color online) Ratio of defect atoms against pumping strength η, 4 ms after the loading of the trap with a uniform ("up") or organized ("down") gas of atoms. The different curves show the approach towards the thermodynamic limit. The parameters are the same as in Fig. 5.

The statistical fluctuations for a finite uniformly distributed atomic ensemble lead to $(N-\delta N)/2$ atoms around the $kz=2n\pi$ and $(N+\delta N)/2$ atoms are around the $kz=(2n+1)\pi$ positions. Taking uniform distributions around the respective antinodes, we have $\Sigma \cos(kz_i) \approx 2\delta N/\pi$ and $\Sigma \cos^2(kz_i) \approx N/2$. The potential difference then reads

$$\Delta E = 2|U_1| = \hbar I_0 \frac{8\delta N}{\pi}(\kappa - N|U_0|/2) = \hbar \frac{4\delta N}{\pi} \frac{\eta^2 g^2}{\kappa \Delta_A^2}. \tag{22}$$

For the final expression in the second line, we considered the far-detuned regime $|\Delta_A| \gg \gamma \sim \kappa \sim g$ and $N|U_0|$, $N\Gamma_0 \ll \kappa$.

The self-organization occurs "instantly" if the trap depth originating from the statistical fluctuations exceeds the average kinetic energy $k_B T$ of the atoms. Using the expectation value of the finite-size fluctuations, $\delta N \approx \sqrt{N}$, we obtain

$$\eta > \eta_\uparrow = \sqrt{\frac{k_B T}{\hbar\kappa}} \frac{\kappa|\Delta_A|}{N^{1/4} g} \frac{\sqrt{\pi}}{2}. \tag{23}$$

Comparison with Eq. (19) gives $\eta_\uparrow = \sqrt{\pi/8} N^{1/4}\ \eta^*$: the functional dependences of the two thresholds on the physical parameters are the same, except for the "anomalous" scaling of $\eta_\uparrow$ with N as the thermodynamic limit is approached.

To check the laboratory time-scale threshold for self-organization (23), we performed simulations with the same physical parameters as in Figs. 5 and 6, starting from uniformly distributed atoms, but this time increasing the atom number with $Ng^4=$const. In Fig. 7, the percentage of defect atoms is plotted as a function of the pumping η. These numerical results confirm that the threshold depends on Ng^4; moreover, the value $\eta_\uparrow = 83\gamma$ from Eq. (23) with $k_B T = \hbar\kappa$ is also consistent with the simulations. In the transition regime, there is a remarkable overlap of the curves corresponding to

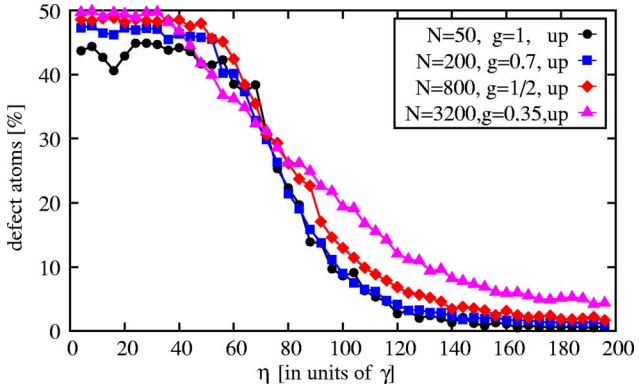

FIG. 7. (Color online) Ratio of defect atoms in the ensemble (measure of the spatial order) as a function of the control parameter η (given in units of γ). There is a clear threshold for self-organization which is independent of the atom number provided Ng^4 is kept constant. Parameters are the same as in Figs. 6 and 5.

various numbers of atoms with keeping Ng^4 constant, indicating that the equilibration time also scales with Ng^4.

The "down" curves of Fig. 6 are invariant with respect to the thermodynamical limit, but the threshold they give is only 50%–80% of the mean-field prediction η^* of Eq. (19). Again, this can be explained with an argument based on the comparison of energy scales. Instead of the statistical fluctuations in the position distribution, we now have a well-defined initial state $\Sigma \cos kz_i = \Sigma \cos^2 kz_i = N$. The threshold $\Delta E > k_B T$ now gives the particularly simple result $\eta > \eta_\downarrow = \eta^*/2$. This is slightly below the "down" curves of Fig. 6; the difference can be attributed to the nonoptimal coupling due to the position spread of the trapped atoms.

In the last curve of Fig. 7, $N=3200$, the atom-cavity coupling g is the smallest parameter, and thus the system does not strictly realize the strong-coupling regime of cavity QED. In fact, self-organization does not depend on strong coupling: small g can be compensated by increasing the number of atoms. We remark that the experimental setup of [21] was also operated out of the strong-coupling regime.

VI. STABLE DEFECT ATOMS

The curve in Fig. 7 corresponding to $N=3200$ deviates slightly from the other data and for large pumping strength it converges to a nonzero value of the defect atoms. In fact, for the parameters chosen there, defect atoms can be stably trapped at the minority sites of the checkerboard of maximally coupled points, which presents another important physical element of the system beyond the capabilities of the simple mean-field theory. In the following we discuss the condition for the appearance of defects and the upper limit on their number.

For the analytical treatment of the defect atoms we use the 1D model of Sec. IV. If the atoms are perfectly self-organized—say, $kz_j = 2n_j\pi$ with integer n_j for every j—then the potential depths of Eqs. (8a) scale with the number of atoms as $U_2 = -N^2 I_0 |U_0|$ and $U_1 = -N2I_0\kappa$. Thus, for large enough N, the $\lambda/2$-periodic potential is dominant and atoms can be trapped in the minority sites. These stable "defect" atoms reduce the superradiant scattering of the self-organized pattern.

How many defects can stably reside in the pattern? For simplicity, we take $N-M$ atoms exactly at $kz = 2n\pi$ and $M < N/2$ "defect" atoms at $kz = (2n+1)\pi$, neglecting the position spread. We then obviously have $\Sigma \cos(kz_i) = N - 2M$ and $\Sigma \cos^2(kz_i) = N$. Substituting this and the prescription (12) for the cavity detuning into Eq. (8a) we obtain

$$U_2 = -(N-2M)^2 |U_0| \hbar I_0, \tag{24a}$$

$$U_1 = -2(N-2M)\hbar I_0 \kappa, \tag{24b}$$

$$I_0 = \frac{|\eta_{\text{eff}}|^2}{[\kappa + N\Gamma_0]^2 + \kappa^2}. \tag{24c}$$

Defect atoms can persist if at every $kz = n\pi$ there is a potential minimum

$$0 < 2|U_2| - |U_1| = 2\hbar I_0 (N-2M)[(N-2M)|U_0| - \kappa],$$

which entails

$$\frac{N}{2} - \frac{\kappa}{2|U_0|} > M. \tag{25}$$

If some defect atoms appear, the rise in their number is limited by the above inequality. In particular, if the left-hand side is negative, there can be no stable defects: the condition for the possibility of stable defects reads

$$N > N_{\text{thr}} = \frac{\kappa}{|U_0|}. \tag{26}$$

Note that this threshold is independent of the pumping strength. The maximum number of defects is limited by

$$M < M_{\max} = \frac{N - N_{\text{thr}}}{2}. \tag{27}$$

Working at large atomic detuning $|U_0| \approx g^2/|\Delta_A|$, we find that defects can appear if the total mode frequency shift due to the atoms exceeds the cavity linewidth:

$$Ng^2 > \kappa |\Delta_A|. \tag{28}$$

This inequality puts a lower bound on the atomic density. Equivalently, it amounts to an upper bound on the atomic detuning Δ_A: to avoid the occurrence of defects a large detuning can be chosen. This $|\Delta_A| \gg Ng^2/\kappa$ is exactly the "far-detuned" limit of the previous sections, used to derive the thresholds η^*, $\eta_\uparrow$, and $\eta_\downarrow$. Likewise, none of the curves in Fig. 6 satisfy Eq. (28). In Fig. 7, however, the curve corresponding to $N=3200$ is above the critical density (28).

For comparison to the full solution of the dynamics, we numerically simulated Eqs. (4) at fixed $\kappa = \gamma/2$, $g = 5\gamma/2$, $\Delta_A = -500\gamma$, and $\eta = 50\gamma$. The number of atoms was varied from 0 to 200; 25 runs with different random seeds were performed for each atom number for a duration of 5 ms. The conditions for self-organization derived in Secs. IV and V give for this parameter setting a threshold atom number $N \gtrsim 10$–40 (for $k_B T = \hbar\kappa - \hbar\gamma$).

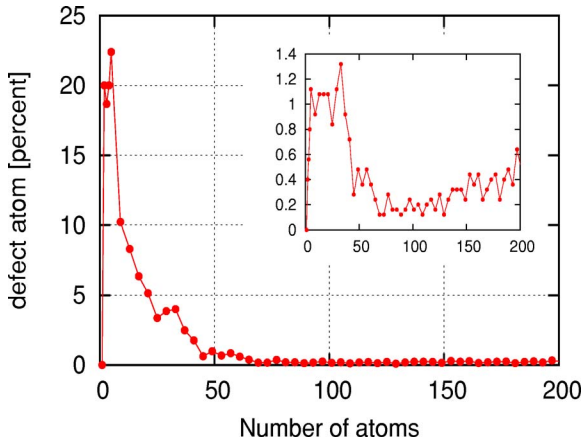

FIG. 8. (Color online) Defect atom ratio 5 ms after loading the trap as a function of the atom number. Each point is an average over 25 runs of the simulation. The inset shows the average number defects. The physical parameters are $\kappa=\gamma/2$, $g=2.5\gamma$, $\Delta_A=-500\gamma$, and $\eta=50\gamma$.

The numerical results presented in Fig. 8 show that the ratio of defect atoms averaged over the 25 trajectories is well below 50%. For small atom numbers this is merely a "finite-size" effect compatible with a balanced binomial distribution. For 15 atoms the defect ratio is still about half; for 18 atoms it is only a quarter of that expected from the uniform distribution. The ratio then drops down to the percent range, indicating stable self-organization, for 50 or more atoms. Concerning the appearance of defect atoms, Eq. (26) gives $N>N_{\mathrm{thr}}\approx 40$. Due to nonperfect bunching, this threshold is shifted to somewhat higher values. The inset of Fig. 8 shows the absolute number of defect atoms after 5 ms, averaged over the runs: the minimum at $N\approx 60$ followed by a rise can be identified with the threshold, which is in accordance with the previous, simple estimate.

The transition from the perfectly ordered phase to the one where defect atoms can be present manifests itself in the statistical properties of the system. As discussed in Sec. III, the appropriate measure of the thermal excitations is the phase-space volume, given by the Heisenberg uncertainty product $\Delta z\Delta p_z/\hbar$. In Fig. 9, this is plotted as a function of the atom number: both the final phase-space volume of individual runs after 5 ms (dots) and the average over these trajectories after 2, 3, 4, and 5 ms (solid lines) are shown. For very few atoms, the phase-space volume is scattered around the value of 13.4, corresponding to uniform spatial distribution and mean kinetic energy $k_BT=\hbar\kappa$. For $N\approx 50$, the decrease of the average phase-space volume and the reducing variance around the mean show that the more stable the self-organized pattern, the less thermally excited the system is. At $N\approx 60$, a broad peak (due to the transition to a double-well potential) heralds the appearance of stable defect atoms. This is followed by a slow but steady increase, which can be attributed to the rising percentage of defects.

To indicate some of the dynamics, Fig. 9 shows the Heisenberg product at earlier times as well: at 2, 3, and 4 ms. The appearance of defect atoms slows down the equilibration process, but the respective curves converge uniformly to the

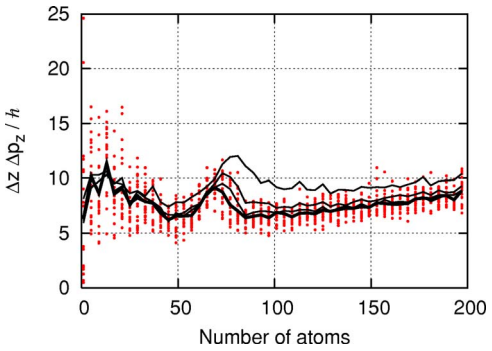

FIG. 9. (Color online) The normalized phase-space volume of the system. Dots represent the values taken at individual trajectories at 5 ms; the thick solid line is their average. The thin lines correspond to the average over the trajectories at 2, 3, and 4 ms. The physical parameters are the same as in Fig. 8.

one obtained at 5 ms. This demonstrates that the cooling time is closely independent of the atom number.

VII. COLLECTIVE EFFECTS IN THE SELF-ORGANIZED PHASE

The most direct evidence of cooperative action is superradiance into the resonator mode that can be measured by detecting the power output from the cavity. In the self-organized checkerboard pattern each atom radiates with the same phase, and so the cavity photon number $|\alpha|^2$ increases quadratically with the number of atoms. This can be observed in the numerical simulations of Eqs. (4), gradually increasing the number of atoms as detailed in the previous section. The cavity photon number is shown on a logarithmic scale in Fig. 10. For many atoms in the cavity ($N>20$) the intensity data are well approximated by the fitted quadratic function $|\alpha|^2=0.08N^2$. The steady-state solution of Eq. (4a) reads

$$|\alpha|^2 = I_0\langle\cos(kz_j)\cos(kx_j)\rangle^2 N^2. \tag{29}$$

If all atoms are perfectly at the antinodes $[\langle\cos(kz_j)\cos(kx_j)\rangle^2=\Theta=\mathcal{B}=1]$, this yields a coefficient of

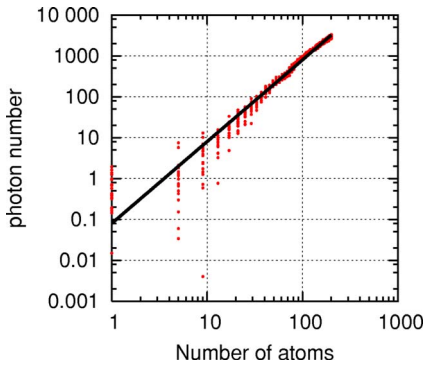

FIG. 10. (Color online) Photon number in the cavity 5 ms after loading. At high atom numbers ($N>20$) the simulation results (dots) are fitted well by a quadratic function (black line), indicating that the atoms scatter cooperatively. The physical parameters are the same as in Fig. 8.

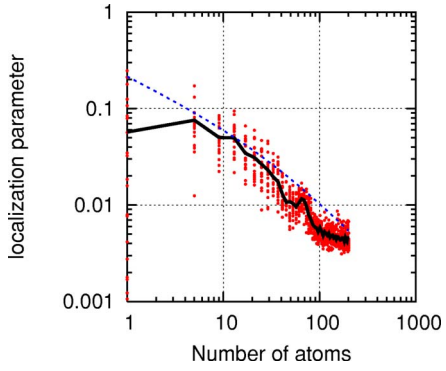

FIG. 11. (Color online) The localization parameter $\mathcal{D}_z = \Sigma_i (k z_i/\pi)^2/N$ measured by the simulation (dots) and averaged over runs (solid black line) shows an overall $1/N$ dependence as a function of the atom number. The dashed line is the approximation of Eq. (31). The physical parameters are the same as in Fig. 8.

0.125. The value from the simulations is 30% below this: the difference can be attributed to the position spread and to the defect atoms.

The superradiance has important effects on the spatial distribution of the atoms about their respective field antinodes. With increasing number of atoms the trap deepens so that the size of the atomic clouds about the antinodes is compressed, as shown in Fig. 11. We note again the appearance of the shoulder at $N \approx 60$ due to the transition into the double-well potential with stable defect atoms. Apart from this, the overall decrease of the localization parameter in the range $N = 10, \ldots, 200$ is proportional to $1/N$. As we show below, this scaling law can be derived by a careful examination of the self-generated trap potential.

We consider one-dimensional motion of the atoms in the limit where they are strongly localized in the vicinity of the antinodes. In this limit of harmonic oscillation the field amplitude in Eq. (4a) is coupled to the atomic positions only through the sum Σz_i^2—i.e., through the localization parameter defined in Eq. (13). It is instructive to introduce new coordinates in the configuration space: the mean radius $r = \sqrt{\Sigma z_i^2/N}$, and a number of $N-1$ angular coordinates φ_j with canonically conjugate momenta $p_{\varphi j} = N m r^2 \dot{\varphi}_j$, these latter decoupled from the field dynamics. Only the radial motion is damped by the cavity cooling mechanism; the angular ones are not. For the coordinate r the potential is composed of the harmonic attraction $\propto r^2$ and a centrifugal repulsion $\propto 1/r^2$. There is a potential minimum and the radius is damped into it by cavity cooling. For large number of atoms the cloud size at an antinode can be simply estimated by the radius at the potential minimum. In this way we discard the role of fluctuations in this coordinate, assuming that the variance is much smaller than the mean.

For a quasistationary field amplitude, the harmonic potential is $m\nu^2 N r^2/2$ with vibration frequency

$$\nu = \sqrt{\frac{\hbar k^2}{m}\left(\frac{|U_0|\eta}{g}|\alpha| + 2|U_0||\alpha|^2\right)}. \tag{30}$$

The angular kinetic energies are of the form $p_{\varphi_j}^2/(2mNr^2)$, $j = 1, \ldots, (N-1)$. The momenta p_{φ_j} can be estimated by their initial value in the unorganized phase, when all degrees of freedom have the same energy $k_B T/2$ and the radius is $r = \lambda/\sqrt{48}$. The potential minimum is just at the radius where the harmonic potential energy equals the sum of the centrifugal energies. Simple algebra leads to the cloud size

$$r^2 \approx \frac{\lambda^2}{8\pi\sqrt{3}}\sqrt{\frac{k_B T}{\hbar|U_0|}}\left(\frac{\eta}{g}|\alpha| + 2|\alpha|^2\right)^{-1/2}, \tag{31}$$

and since $|\alpha|^2 \propto N^2$, the $1/N$ law for the localization parameter follows. Altogether, the increase in atom number results in a smaller cloud size in the vicinity of the antinodes, a very important virtue of the collective atomic action. This compression is limited by the dipole-dipole interaction of the atoms near the same antinode, which effect was not taken into account in the present model.

VIII. CONCLUSION

A dilute cloud of noninteracting cold atoms in a high-Q cavity can undergo a phase transition if driven from the side by a laser sufficiently red detuned from an atomic resonance. Increasing the laser power above a threshold the atoms self-organize into a lattice so as to scatter most effectively into the cavity mode. In this way the atoms minimize their energy in the optical potential generated from the interference pattern of the cavity and pump field. Under proper conditions the atoms are cooled in this process, giving long-term stability to the pattern.

The phenomenon has been previously seen in simulations, and strong evidence was found in experiments [21], but threshold, scaling, and efficiency of the effect with atom number, cavity parameters, and system size remained unclear. Here we gave a thorough analytical discussion of the effect. A continuous density approach allowed us to derive analytical formulas for the critical pump power as a function of atom number and cavity volume and showed that the effect should persist if one scales up the volume at fixed atomic density, i.e.—$Ng^2 = \text{const}$. Numerical simulations of the evolution for finite durations revealed a hysteresis between the ordered and homogeneous density phases on varying the control parameter—i.e., the pumping strength. This shifts the observable threshold in the pumping strength, which then scales with Ng^4. We still have a cooling mechanism for large numbers of any type of optically polarizable particles.

The system is composed of noninteracting atoms that communicate via a commonly coupled, single cavity mode. The cavity component of the system plays a multiple role. First, the binding energy of the ordered phase is stored in the superradiantly enhanced field intensity of this single mode. Next, as an attractive feature of this system, the outcoupled field intensity directly serves as a possibility of time-resolved monitoring of the formation of the ordered phase. Note that in setups without resonator, the uncontrolled scattered field can lead to a binding of micrometer-sized particles in an ordered pattern in liquid [42,43]. In the cavity scheme, finally, the viscous motion is provided by the dynamically coupled single-mode cavity field. Apart from the geometry,

this is also a distinctive feature with respect to CARL.

From the laser cooling point of view, the picture is complicated by the phase transition. The appropriate measure of the cooling efficiency is the phase-space volume occupied by the system. The self-organization process reduces this volume below that of a system at the cavity cooling limit with uniform spatial distribution. Moreover, the steady state is established within milliseconds, and this is closely independent of the number of atoms in the cloud (numerical simulations confirm this up to a few hundreds of atoms). Collective cooling was previously known only for the stochastic cooling method [44] and for common vibrational modes of trapped particles [45]. The collective behavior strongly improves the localization; i.e., the size of the atom cloud pieces at the trapping sites is proportional to the inverse of the atom number.

This work could be extended to various directions. First of all, the numerical simulations should confirm some of the statements of the present paper on a larger range of the atom number or on a longer time scale (e.g., the dependence of the hysteresis on the duration of the evolution). Our prescription for the pump-cavity detuning Δ_C in Eq. (12) is probably impractical in the limit of large atom numbers, as one has to go closer to the resonance in order to initiate the self-organization. Next, the maximum achievable densities cannot be determined in the present model as some of the limiting factors were omitted—e.g., vacum-mediated dipole-dipole interactions between the atoms, the eventual superradiant enhancement of the spontaneous scattering into lateral directions, etc. In extremely good cavities, quantum effects in the motion of the atoms begin to play an important role [46,47], which was not studied here. Finally, the nature of the phase transition is strongly determined by the geometry of the cavity mode: the possible trapping sites are defined by the antinodes of the cavity mode and the transverse pumping field. This situation can be essentially modified in a cavities with different geometry—e.g., ring or confocal resonator.

ACKNOWLEDGMENTS

We thank Walter Rantner for useful discussions and Zoltán Kurucz for reading the manuscript. This work was supported by the National Scientific Fund of Hungary (Contract Nos. T043079 and T049234), the Bolyai Program of the Hungarian Academy of Sciences, and by the Austrian FWF SFB P12.

[1] H. J. Metcalf and P. van der Straten, *Laser Cooling and Trapping* (Springer, New York, 1999).
[2] P. Meystre, *Atom Optics* (Springer, New York, 2001).
[3] Y. Castin, in *Coherent Atomic Matter Waves*, Lecture Notes of Les Houches Summer School, edited by R. Kaiser, C. Westbrook, and F. David (EDP Sciences and Springer-Verlag, Berlin, 2001), pp. 1–136.
[4] O. Morice, Y. Castin, and J. Dalibard, Phys. Rev. A **51**, 3896 (1995).
[5] A. Lagendijk, B. Nienhuis, B. A. van Tiggelen, and P. de Vries, Phys. Rev. Lett. **79**, 657 (1997).
[6] G. Labeyrie, E. Vaujour, C. A. Müller, D. Delande, C. Miniatura, D. Wilkowski, and R. Kaiser, Phys. Rev. Lett. **91**, 223904 (2003).
[7] G. Labeyrie, D. Delande, C. A. Müller, C. Miniatura, and R. Kaiser, Phys. Rev. A **67**, 033814 (2003).
[8] D. W. Sesko, T. G. Walker, and C. E. Wieman, J. Opt. Soc. Am. B **8**, 946 (1991).
[9] C. J. Hood, T. W. Lynn, A. C. Doherty and A. S. P. H. J. Kimble, Science **287**, 1447 (2000).
[10] P. W. H. Pinkse, T. Fischer, P. Maunz, and G. Rempe, Nature (London) **404**, 365 (2000).
[11] P. Horak, G. Hechenblaikner, K. M. Gheri, H. Stecher, and H. Ritsch, Phys. Rev. Lett. **79**, 4974 (1997).
[12] P. Domokos and H. Ritsch, J. Opt. Soc. Am. B **20**, 1098 (2003).
[13] P. Maunz, T. Puppe, I. Schuster, N. Syassen, P. W. H. Pinkse, and G. Rempe, Nature (London) **428**, 50 (2004).
[14] S. Nussmann, K. Murr, M. Hijlkema, B. Weber, A. Kuhn, and G. Rempe, e-print quant-ph/0506067.
[15] P. Münstermann, T. Fischer, P. Maunz, P. W. H. Pinkse, and G. Rempe, Phys. Rev. Lett. **84**, 4068 (2000).
[16] A. T. Black, J. K. Thompson, and V. Vuletić, J. Phys. B **38**, S605 (2005).
[17] J. K. Asboth, P. Domokos, and H. Ritsch, Phys. Rev. A **70**, 013414 (2004).
[18] T. Fischer, P. Maunz, T. Puppe, P. W. H. Pinkse, and G. Rempe, New J. Phys. **3**, 11.1 (2001).
[19] P. Horak and H. Ritsch, Phys. Rev. A **64**, 033422 (2001).
[20] P. Domokos and H. Ritsch, Phys. Rev. Lett. **89**, 253003 (2002).
[21] A. T. Black, H. W. Chan, and V. Vuletić, Phys. Rev. Lett. **91**, 203001 (2003).
[22] D. Kruse, C. von Cube, C. Zimmermann, and P. W. Courteille, Phys. Rev. Lett. **91**, 183601 (2003).
[23] B. Nagorny, T. Elsässer, and A. Hemmerich, Phys. Rev. Lett. **91**, 153003 (2003).
[24] T. Elsässer, B. Nagorny, and A. Hemmerich, Phys. Rev. A **69**, 033403 (2004).
[25] S. Slama, C. von Cube, B. Deh, A. Ludewig, C. Zimmermann, and P. W. Courteille, Phys. Rev. Lett. **94**, 193901 (2005).
[26] R. Bonifacio, L. DeSalvo, L. M. Narducci, and E. J. D'Angelo, Phys. Rev. A **50**, 1716 (1994).
[27] M. Perrin, G. L. Lippi, and A. Politi, Phys. Rev. Lett. **86**, 4520 (2001).
[28] G. R. M. Robb and B. W. J. McNeill, Europhys. Lett. **62**, 217 (2003).
[29] J. Javaloyes, M. Perrin, G. L. Lippi, and A. Politi, Phys. Rev. A **70**, 023405 (2004).
[30] C. von Cube, S. Slama, D. Kruse, C. Zimmermann, P. W. Courteille, G. R. M. Robb, N. Piovella, and R. Bonifacio, Phys. Rev. Lett. **93**, 083601 (2004).

[31] G. R. M. Robb, N. Piovella, A. Ferraro, R. Bonifacio, P. W. Courteille, and C. Zimmermann, Phys. Rev. A **69**, 041403(R) (2004).
[32] J. A. Sauer, K. M. Fortier, M. S. Chang, C. D. Hamley, and M. S. Chapman, Phys. Rev. A **69**, 051804(R) (2004).
[33] D. Schrader, S. Kuhr, W. Alt, M. Müller, V. Gomer, and D. Meschede, Appl. Phys. B: Lasers Opt. **73**, 819 (2001).
[34] D. Schrader, I. Dotsenko, M. Khudaverdyan, Y. Miroshnychenko, A. Rauschenbeutel, and D. Meschede, Phys. Rev. Lett. **93**, 150501 (2004).
[35] P. Domokos, P. Horak, and H. Ritsch, J. Phys. B **34**, 187 (2001).
[36] P. Domokos, A. Vukics, and H. Ritsch, Phys. Rev. Lett. **92**, 103601 (2004).
[37] G. Hechenblaikner, M. Gangl, P. Horak, and H. Ritsch, Phys. Rev. A **58**, 3030 (1998).
[38] A. C. Doherty, T. W. Lynn, C. J. Hood, and H. J. Kimble, Phys. Rev. A **63**, 013401 (2000).
[39] V. Vuletić, H. W. Chan, and A. T. Black, Phys. Rev. A **64**, 033405 (2001).
[40] S. J. van Enk, J. McKeever, H. J. Kimble, and J. Ye, Phys. Rev. A **64**, 013407 (2001).
[41] K. Murr, J. Phys. B **36**, 2515 (2003).
[42] M. M. Burns, J. M. Fournier, and J. A. Golovchenko, Phys. Rev. Lett. **63**, 1233 (1989).
[43] W. Singer, M. Frick, S. Bernet, and M. Ritsch-Marte, J. Opt. Soc. Am. B **20**, 1568 (2003).
[44] M. G. Raizen, J. Koga, B. Sundaram, Y. Kishimoto, H. Takuma, and T. Tajima, Phys. Rev. A **58**, 4757 (1998).
[45] A. Beige, P. L. Knight, and G. Vitiello, New J. Phys. **7**, 96 (2005).
[46] S. Zippilli and G. Morigi, Phys. Rev. Lett. **95**, 143001 (2005).
[47] A. Vukics, J. Janszky, and P. Domokos, J. Phys. B **38**, 1453 (2005).